RSC Advances

ROYAL SOCIETY OF CHEMISTRY

www.rsc.org/advances

Solvothermal Synthesis and Visible-light-driven Photocatalytic Degradation for Tetracycline of Fe-doped $SrTiO_3$

Ping Li[a], *Chunbo Liu*[a], *Guoling Wu*[a], *Yang Heng*[b], *Shuang Lin*[a], *Ao Ren*[a], *Kehan Lv*[c] *Lisong Xiao*[a], *Weidong Shi*[a,*]

[a] School of Chemistry and Chemical Engineering, Jiangsu University, Xuefu Road 301, Zhenjiang, 212013, P. R. China.

[b] School of Hydraulic, Energy and Power Engineering, Yangzhou University, Yangzhou, 225100, P. R. China

[c] School of Petrochemical Engineering, Changzhou University, Changzhou, 213100, P. R. China

[*]Corresponding author: Tel.: +86 511 8879 0187 fax. : +86 511 8879 1108

E-mail address: swd1978@ujs.edu.cn (W. Shi)

ABSTRACT

In this paper, Fe-doped $SrTiO_3$ (FSTO) photocatalysts were successfully prepared via a facile solvothermal method, and the photocatalytic activity for degrading tetracycline (TC) under visible light irradiation was examined. It was found that doping Fe^{3+} into the lattice of $SrTiO_3$ resulted in the formation of new absorption bands in visible light region and the energy band gap decreased from 3.2 eV to 2.6 eV with the doping amount of Fe^{3+} from 0 to 5 wt%. The photocatalytic experimental results indicated that the as-prepared FSTO photocatalysts show extremely high enhancement of TC degradation ratio over the pure $SrTiO_3$ under visible light irradiation. Specially, the sample of FSTO doped with 3% Fe exhibited the highest TC degradation ratio (71.6%) in 80 min, which is mainly attributed to the narrowed gap brought by appropriate Fe^{3+} doping. This work suggests that the doping method should be applicable for exploiting other efficient visible-light-driven photocatalysts with wide band gap semiconductors.

Keywords: Fe-doped $SrTiO_3$; visible light; tetracycline; photocatalyst

1. Introduction

In recent years, the utilization of antibiotics in the pharmaceutical therapies and agricultural husbandry to reduce the morbidity of infectious diseases becomes more and more widely. However, these antibiotics are very difficult to be metabolized completely and the ultimate impact of antibiotics in the environment is the appearance of multi-resistant bacterial strains that can no longer be treated with the known drugs presently. Thus, the antibiotics resided in the ecological environment have become one of the most concerned issues due to their potential adverse effects on human beings[1-5]. Tetracycline (TC) is one of the largest use of antibiotics currently, and it has been established that their excessive accumulation can produce arthropathy, nephropathy, central nervous system alterations, spermatogenesis anomalies, possible mutagenecity and photosensitivity in human beings [3, 6, 7]. Hence, it is very important to develop efficient treatment technologies to remove antibiotics left in the ecological environment. All sorts of technologies have been used to remove antibiotics, such as UV/H_2O_2 process, biodegradation, electrochemical methods, photocatalysis [8, 9]. With great promise, photocatalysis has shown the high efficiency in oxidizing organics, high degradation rate, low cost and operation-simplicity [10]. Recently, several studies on the high-efficiency photocatalytic degradation of TC by semiconductor-based (such as TiO_2, ZnO, and $SrTiO_3$) photocatalysts have been reported[11-13]. But, most of them are UV-light driven rather than visible-light driven. Hence, it is highly desirable to develop visible-light-responsive photocatalysts with high efficiency for TC degradation.

Titanates or titanium-containing oxides have been used for a variety of solar energy harvesting and environmental applications such as photoelectrochemical synthesis of carbon-neutral solar fuels and removal of organic pollutants owing to

their remarkable photostability, nontoxicity, piezoelectric dielectric, and cost effectiveness [14-16]. Unfortunately, titanates suffer from poor visible light absorption because of their high intrinsic band gap structure. Recently, to realize the visible-light adsorption of material, introducing foreign elements into the lattice of semiconductor is considered to be one of the effective strategies to enlarge the adsorption region[17-19]. In principle, changing the stoichiometry or doping with a different valence state cation can transform the electronic properties and catalytic properties [17]. It was reported that doping of some metals such as Co^{2+}, Ru^{3+}, Fe^{3+}, Cr^{3+} and Mn^{3+} incorporated into $SrTiO_3$ (STO) to create a new donor or acceptor level in the band structure lead to an optical absorption shift to visible light [9, 13, 20, 21]. Based on the above-mentioned reports, Fe maybe is a better suitable doping element, in addition to the same coordination number of 6, Fe^{3+} (0.79 Å) and Ti^{4+} (0.75 Å) have similar ionic radius, doping Fe^{3+} into STO also can lead to the formation of impurity energy level between the conduction band and valence band of STO, which acts as a trap for the electron-hole pairs and consequently inhibits their recombination, and doping Fe^{3+} can also increase the electro-catalytic properties of materials while Fe is a transition metal [13]. However, to the best of our knowledge, there have been few reports on the synthesis of Fe-doped $SrTiO_3$ (FSTO). More importantly, the as-obtained FSTO samples are always focused on the resistive transition, polaron dynamics and scaling behavior[22-30], studying on the visible light degrading for antibiotics have not been reported to date.

Herein, we report the synthesis of STO and FSTO nanospheres by a facile solvothermal method and the as-prepared samples are employed for the first time as the photocatalyst to photodegrade TC under visible light. Compared to pure STO sample, the FSTO samples exhibit excellent visible-light-driven photodegradation of

TC. Specially, the sample of FSTO doped with 3% Fe exhibited the highest TC degradation ratio (71.6%) in 80 min. Finally, a possible photocatalytic reaction mechanism of FSTO was proposed based on the experimental results.

2. Experimental

2.1. Materials

Tetra-n-butyl titanate, ethylene glycol, $Sr(NO_3)_2$, NaOH, $Fe(NO_3)_3 \cdot 9H_2O$ and ethanol were purchased from Aladdin (Shanghai, China). All the reagents are analytically grade and used without further purification.

2.2. Catalysts synthesis

For the synthesis of STO nanospheres, tetra-n-butyl titanate (0.9mL) was added dropwise into ethylene glycol (EG, 25mL) under magnetic stirring at room temperature. The suspension was added into 25mL of an aqueous solution containing $Sr(NO_3)_2$ (4.9mmol), and then NaOH (0.20g) was added into the mixture under vigorous stirring for 15 min. Thereafter, the resulting mixture was transferred into a Teflon-lined stainless steel of 50 mL capacity, and the solvothermal route was carried out at 150 ℃ for 18 h. After cooling to room temperature naturally, the white precipitate was collected by centrifugation and thoroughly washed with deionized water and ethanol several time, and dried at 60 ℃ in vacuum for 12 h to obtain pure STO.

The samples FSTO with X= 0.015, 0.025, 0.03, 0.04 and 0.05 (abbreviated as FSTO:X) were prepared totally the same except that $Fe(NO_3)_3 \cdot 9H_2O$, acting as the source of Fe(III), was weighed to give a molar fraction of Fe relative to Ti is X and added to the suspension. Subsequently, the obtained FSTO were ground into a fine powder using an agate mortar and pestle for the preparation of FSTO nanocomposites.

2.3. Characterization

Powder X-ray diffraction (XRD) patterns were obtained on a D/MAX-2500 diffractometer (Rigaku, Japan) using Cu Kλ radiation source (λ= 1.54178 Å) at a scan rate of 5° min^{-1} to determine the crystal phase of the obtained samples. X-ray photoelectron spectroscopy (XPS) data were obtained by a Thermo ESCALAB 250X (America) electron spectrometer using 150 W Al Kλ radiations. Energy dispersive X-ray spectra (EDX) images were collected on an F20 S-TWIN electron microscope (Tecnai G2, FEI Co.), using a 200 kV accelerating voltage. Scanning electron microscopy (SEM) images were collected on an S-128 4800 field emission SEM (FESEM, Hitachi, Japan). Transmission electron microscopy (TEM) and high-resolution TEM (HRTEM) also has been used to characterise the samples. HAADF-STEM mapping analyses were collected on an F20 S-TWIN electron microscope (Tecnai G2, FEI Co.), using a 200 kV accelerating voltage. UV–vis diffused reflectance spectra of the samples were obtained from a UV2550UV–vis spectrophotometer (Shimadzu, Japan). $BaSO_4$ was used as a reflectance standard. The photoluminescence properties of the obtained samples were measured on a Perkin-Elmer LS 55 luminescence spectrometer. Total organic carbon (TOC) analyses were conducted on a multi N/C 2100 (Analytik Jena AG, Germany) TOC analyzer.

2.4. Photocatalytic degradation of TC

The photodegradation properties of STO and FSTO were further evaluated by monitoring the photodegradation of a widely used antibiotic, namely tetracycline, under visible-light irradiation (300W xenon lamp with a cutoff filter of 420 nm). A total of 0.1 g of catalysts was added to 100 mL of tetracycline solution (10mg/L). Before irradiation, the suspensions were magnetically stirred in the dark for 30 min until the stability of an adsorption-desorption equilibrium between the photocatalyst

and TC was reached. The supernatant liquid was collected and analyzed by recording the characteristic absorption of tetracycline (357 nm) using the UV-vis spectrometer. The photocatalytic degradation ratio (DR) was calculated by the following formula:

$$DR = (1 - A_i / A_0) \times 100\%$$

A_0 is the initial absorbance of TC when reached absorption equilibrium, while A_i is the absorbency after the sampling analysis.

2.5. Kinetics of photocatalytic degradation of TC

With the Langmuir-Hinshelwood mechanism, the evaluation of the kinetics of the degradation of TC follows an apparent first order kinetics equation [31] (eq 1):

$$\ln(C_0 / C) = kKt \approx k_{app} t \qquad (1)$$

Where C is the concentration of reactant (mg/L), and C_0 is the initial concentration at t= 0. The apparent rate constant (k_{app}) has been chosen as the basic kinetic parameter for the different photocatalysts since it enables one to determine a photocatalytic activity independent of the previous adsorption period in the dark and the concentration of solute remaining in the solution

3. Results and discussion

3.1. Structure and morphology

The X-ray diffraction (XRD) patterns of the pure STO and FSTO are shown in Fig. 1a. As it reveals, the peaks observed at 2θ values of 22.8°, 32.2°, 40°, 46.5°, 58°, 68° and 77.2° in this pattern are reflections of STO according to the JCPDS Card No. 35-0734 [32]. Apparently, there are no peaks to Fe^{3+} phases were identified, probably due to the low Fe^{3+} concentrations in STO matrix. Another explanation is, for a coordination number of 6, Fe^{3+} (0.79 Å) and Ti^{4+} (0.75 Å) have similar ionic radius, so Fe^{3+} may substitute Ti^{4+} in the STO lattice [13]. Fig. 1b shows the EDX image

of the sample FSTO: 0.03, in which the signals of Sr, Ti, O and Fe can be clearly observed. No other signals can be observed in the spectrum, which indicated that the elementary composition of FSTO sample is pure.

Analyses of SEM images are depicted in Fig. 2. As shown in Fig. 2a, we can see the morphology of STO is nanosphere with uniform and good-dispersion. The morphology of FSTO is shown in Fig. 2d, we can see the FSTO is not uniform and have different sizes. The magnified TEM image (Fig. 2b，c) provides a better view of these particles, from which the size of STO nanosphere can be identified as 300 nm and that of FSTO ranging from 100nm to 300nm. Therefore, doping may affect the morphology of the photocatalysts. The morphology and structure of STO and FSTO particles was further studied by using the high-resolution TEM images (HRTEM). The HRTEM images (Fig. 2e, f) were recorded on the surface of nanospheres. The lattice fringes on the pure STO have interplanar spacing d = 0.276 nm (Fig. 2e), which perfectly corresponds to the (1 1 0) plane of STO, and that of FSTO is 0.275 nm (Fig. 2f), with little difference between pure STO. [33] Combined with SEM and TEM images, it can be drawn that doping can affect the morphology of materials, which is not just on the macroscopic morphology, but also the interplanar spacing.

To further determine the composition and element distribution of the FSTO sample, the HAADF-STEM is operated to show the intensity of Sr, Ti, O and Fe signals. The HAADF-STEM images of FSTO: 0.03 are shown in Fig. 3. The maps of Sr, Ti, O and Fe are also given in the Fig. 3, which have the same shape and locations, giving solid evidence that Fe^{3+} has been successfully doped into the STO lattices, this is consistent with the results of the XRD and EDX.

3.2. X-ray photoelectron spectra (XPS)

More evidence is given by the XPS spectra of sample SFTO: 0.03, as shown in

Fig. 4. In the full range XPS spectrum (Fig. 4a), the signals of Sr, Ti, O, and Fe with different states can be clearly observed, which means the definite existence of $SrTiO_3$ and Fe^{3+}. The C element could be ascribed to the adventitious carbon-based contaminant, and the binding energy for C 1s peak at 284.6 eV was used as the reference for calibration. In the high-resolution spectrum of Ti 2p of SFTO: 0.03 (Fig. 5b), one peak exists at 458.4 eV, which is ascribed to the Ti 2p3/2. And in the Fig. 5c, the peak exists at 132.8 eV, which is ascribed to the Sr 3d5/2. In the high-resolution spectrum of Fe 2p of SFTO: 0.03 (Fig. 5d), the two peaks exist at 720.3 eV and 710.3 eV are ascribed to Fe 2p 1/2 and Fe 2p 3/2 respectively. The proportion of elements is shown in Table 1, it is seen that the atomic ratio of Fe is 1.0%, which is smaller than the initial raw material ratio (3%). This is maybe because XPS is a surface chemical analysis technique, the depth of its sampling is ranging from 2nm to 5nm, so it provides the elements content on the surface, which is very different from the bulk composition. Another reason maybe is the source of Fe(III) does not participate in the reaction completely.

3.3. UV−vis absorption spectra

Fig. 5 displays the UV-vis absorption spectra of pure STO and FSTO. As shown in Fig. 5a, with the increasing amount of Fe^{3+}, there is an enhanced absorbance in the visible-light region (λ>420 nm). We can also observe a color change of the samples, that is, from white to yellow (inset in Fig. 5a). The absorption edge extends visible region to about 600nm. It has reported that doping Fe^{3+} into TiO_2 may lead the generation of the impurity energy level between the conduction band and valence band of TiO_2 [34]. In the energy level of Fe^{3+}, the excited electrons could transfer to the conduction band of TiO_2, which lead an absorption in the visible light region. So the absorption in the visible light as shown in Fig. 5a is owing to the excited electrons

from the isolated energy level which produced by Fe^{3+} to the conduction band of FSTO. The energy band gap of FSTO could be calculated using band gap energy relation of Eg (eV) =1240 / λ (nm), where λ □is absorption edge and Eg is energy band gap of FSTO. As shown in Fig. 5b, by changing the Fe^{3+} doping amount from 0 to 0.05, the energy band gap can be precisely controlled from 3.2 eV to 2.6 eV.

3.4. Photocatalytic degradation of TC

In our work, the experiments of the catalytic activities on pure STO and FSTO photocatalysts with different Fe proportion were carried out in 80 min under visible light irradiation (λ>420 nm) for comparison, as shown in Fig. 6, and we found the FSTO photocatalysts show excellent enhancement in the photodegradation of TC under visible light irradiation. Fe^{3+} proportion has a crucial influence on the photocatalytic activities of FSTO photocatalysts. Even a very small amount (0.015) of Fe^{3+} contributes a huge enhancement to the photocatalytic performance. As shown in Fig. 6, the pure STO photocatalysts do not exhibit degradation ratio under visible light, which due to wide energy gap of 3.2 eV. Only, with the existence of Fe^{3+} (0.015), the DR of FSTO: 0.015 sample is enhanced to 61.3%, which shows excellent enhancement compared to pure STO sample. The trend of DR is well increased as the proportion of Fe^{3+} increased from FSTO: 0.015 to FSTO: 0.03 and the FSTO: 0.03 sample shows the highest DR (71.6%). The photocatalytic DR of TC decreases rapidly as the Fe^{3+} proportion over 0.03. The FSTO: 0.05 sample shows the lowest DR of 52.5% among all the FSTO photocatalyst samples, but it is still much higher than that of the STO sample.

3.5. The Kinetic study of photocatalytic degradation of TC

In order to further illustrate the photocatalytic reaction, the kinetic behavior is discussed. The photodegradation reaction kinetics of TC can be described by a

Langmuir−Hinshelwood model according the report [35]. Fig. 7a shows the $\ln(C_0/C)$ versus time interval and the apparent rate constant values for photodegradation of the TC solution over different photocatalysts in 80 min under visible light irradiation. As shown in Fig. 7a, we can draw the conclusion that the SFTO photodegrade TC under visible light irradiation comply with the first-order kinetics. The value of k_{app} gives an indication of the activity of the photocatalyst, as shown in Fig. 7b. Apparently, for the TC photodegradation the rate constants for SFTO: 0.03 sample exhibits the highest rate constant of about 0.197 min^{-1}, which is consistent with the result of the photocatalytic degradation of TC.

3.6. Photoluminescence spectra (PL) analysis

It is well acknowledged that the PL emission intensity is related to the recombination of electrons and holes. The lower PL emission intensity shows the less of an opportunity for electron-hole pairs' recombination, the more effectively migration of charge-carriers, thereby [36]. The intensity and wavelength of PL spectrum are sensitive to the doping of aliovalent ions [15]. The measurement was conducted at the excitation wavelength of 281 nm with PMT voltage of 500 V and the PL emission maximum of FSTO samples are both at 382 nm. As shown in Fig. 8 the PL emission intensity of FSTO: 0.03 is lower than that of FSTO: 0.015. This means that the FSTO: 0.03 has a lower recombination of photoinduced electron-hole pairs, when the recombination rate decreases, more photo-generated charge carriers can participate in the photochemical transformation, resulting in the enhancement of photocatalytic activity. With increasing the Fe^{3+} concentration, the PL intensity decreases and reaches a minimum value at the amount is 0.03. When the Fe^{3+} concentration exceeds this value, the PL intensities increase remarkably. The reason is that the Fe^{3+} incorporated into the STO can act as the electron-trapped agent to promote the

electron-hole separation at low doping concentration, while as the recombination center when the Fe^{3+} concentration exceeds the threshold and begins to aggregate [37].

3.7. Total organic carbon (TOC) analyses

To proof the degradation of the TC is owing to the photocatalysis rather than the physical adsorption, the TOC analyses were studied. As shown in Fig. 9a, the reduction of TC with the photocatalyst of the FSTO: 0.03 under visible light. In 80 min, the remove of the TC is reached 42.5%, lower than that of the DR. The reasonable reason is that the degradation curve data were measured after the photocatalyst separation step by centrifugation [38]. As shown in Fig. 9b, the TOC trend of the TC is similar to that of photo degradation represent that our experiments of the photocatalysis successfully and correctly evaluated the DR of the TC. Meanwhile, the trend of the TOC means our photocatalysts have enormous potential of decomposition of TC [39]. Besides, we can also conclude that there are maybe many of intermediate products.

3.8. High-performance liquid chromatography (HPLC) analyses

The process of degrading TC under visible light irradiation was also researched using the research method of HPLC analyses. Fig. 10a shows a not symmetrical peak of TC at the start. As time goes on, the peak of TC is weaken gradually, and nearly disappears within 80 min. Peak area represents the relative concentration of a substance in a solution, as shown in Fig. 10b, the concentration of TC is decreased, so we can be found that the degradation of TC under visible light irradiation is clipping and efficient with the photocatalyst is FSTO: 0.03.

3.9. Active species trapping experiments

A series of active species trapping experiments were conducted to further investigate the photocatalytic degradation mechanism of TC. Fig. 11 shows the results

of adding different radical scavengers over the FSTO: 0.03 photocatalysts under visible-light irradiation. When triethanolamine (TEA) [40-44] traps for h^+ is added into the reaction system, the photodegradation is greatly restrained compared to the reaction without radical scavengers. It can be easily found that the addition of TEA in the catalytic system leads to a 50% decrease to the photocatalytic degradation rate of TC under FSTO: 0.03. A similar and obvious suppression phenomenon is also observed with the benzoquinone(BQ) [43] scavenger for $\cdot O_2^-$. Therefore, it can be concluded that h^+ and $\cdot O_2^-$ are the main active species of FSTO: 0.03 in aqueous solution under visible light irradiation. However, when 10 mL of iso-propanol (IPA) [45] for ·OH is added into the reaction system, the degradation of TC is slightly lower to the reaction without radical scavengers, so the ·OH indicating that ·OH plays a minor role for TC degradation. On the contrary, the photocatalytic degradation of TC obviously increased with the addition of $AgNO_3$ for e^- [40-44]. The increase suggests that the scavenger of e^- has less of an opportunity for electron-hole pairs' recombination and facilitates the production of more holes.

3.10. Reactive species in the catalytic system

In order to determinate the presence of ·OH and $\cdot O_2^-$ effectively and intuitively, ESR experiments were carried out under visible light.[45] FSTO: 0.03-H_2O/DMPO and FSTO: 0.03-CH_3OH/DMPO were prepared by the following experimental process: 10 mg samples and 40 μL DMPO were dissolved in 0.5 mL deionized water and stirred for 5 min (solution A) and the solution B were prepared the same except the water was changed by CH_3OH. Solution A was used as the detection of hydroxyl radicals (DMPO-·OH), and solution B was used as the detection of superoxide radicals (DMPO-$\cdot O_2^-$). As shown in Fig. 12a, it can be seen that the strong characteristic peaks corresponding to DMPO-·OH adduct are observed for the FSTO: 0.03 samples. From

Fig. 12b, it is clear that the characteristic peaks of the DMPO-$\cdot O_2^-$ adducts are observed in the ESR patterns for the FSTO: 0.03 samples. This proves that the $\cdot O_2^-$ have been produced during the process of photocatalytic reaction. The number of characteristic peaks of the DMPO-$\cdot O_2^-$ adducts is four, which is because the solution B is neutral (PH=7) [46]. If the solution is acid, then the number will be six, and this is because their hyperfine splitting peaks are not the same [47]. According to the ESR analyses, we can make the conclusion that the presence of ·OH and $\cdot O_2^-$, furthermore, from the active species trapping experiments, we suggested that $\cdot O_2^-$ and h^+ also played a major role in the photocatalytic degradation of TC, and the ·OH is in a weaker position [48].

On the basis of the experimental results, doping Fe^{3+} into STO can lead to the formation of impurity energy level between the conduction band and valence band of STO [13]. So we can have consideration for that the new structure of FSTO may easily generate electronics and holes to the surface of nanomaterials and initiate the photocatalytic reactions in the visible region, we can come to the conclusion that the possible mechanism is [16], as shown in Scheme 1. Firstly, the photocatalysts generate electron-hole pairs since the electron come to conduction band from impurity energy level; secondly, in the conduction band, the generation of $\cdot O_2^-$ radicals due to the electron reacts with the oxygen molecule; meanwhile, the h^+ will going to decompose the pollutant target and a small amount of h^+ will going to produce ·OH to degrade TC.

The trend of DR is well increased as the proportion of Fe^{3+} increased from STO to FSTO: 0.03. The FSTO: 0.03 samples show the highest DR (71.6%) among all the samples. The photocatalytic DR of TC decreases rapidly as the Fe^{3+} proportion over 0.03. The FSTO: 0.05 samples show the lowest DR of 45.2% among all the FSTO

photocatalyst samples. The decrease of DR of photocatalysts with relatively high (over 0.03) Fe^{3+} proportion may also result from the Fe^{3+} ions have been successfully doped into the STO crystal lattice by substituting Ti^{4+}, accompanying the generation of active sites in STO. The active sites at appropriate content can effectively capture the electrons or holes and prolong the lifetime of photogenerated charges thereby increasing the photo-quantum efficiency. But, with Fe^{3+} ion increases, excessive active sites can act as recombination centers of photogenerated electrons and holes, thus reducing the photocatalytic activity of the powders [37]. As a consequence, the suitable Fe^{3+} proportion is crucial for optimizing the photocatalytic activity of FSTO composite photocatalysts.

4. CONCLUSION

In conclusion, the STO and FSTO photocatalysts were successfully synthesized by the hydrothermal method. The XRD was assigned to the pure STO, and no peaks to Fe^{3+} phases were identified, probably due to the low Fe^{3+} concentrations in STO matrix. The EDX and XPS spectra of the photocatalysts were assigned to the existence of Fe^{3+}. From the UV-vis spectra, by changing the Fe^{3+} doping amount from 0 to 5%, the energy band gap can be precisely controlled from 3.2 eV to 2.6 eV. And as PL spectrum shows, the PL emission intensity of FSTO: 0.03 is lower than that of other FSTO samples and pure STO. This means that the FSTO: 0.03 has a lower recombination of photoinduced electron-hole pairs, which improved the photocatalytic activity under visible light. From the photocatalysis experiment, we can also draw a conclusion that the FSTO: 0.03 has the highest photodegradation of TC reached to 71.6%. In addition, the TOC, HPLC, active species trapping experiments analyses and ESR analyses were conducted to proof the photocatalysts react with TC under h^+ and $\cdot O_2^-$ as the main active species to produce CO_2 and H_2O or other inorganic molecules.

Acknowledgments

The authors are grateful for National Natural Science Foundation of China (21276116, 21301076, 21303074 and 21201085), Natural science foundation of Jiangsu Province (BK20131257, BK2012294), Special Financial Grant from the China Postdoctoral Science Foundation (2013T60501), Open Project of the Key Laboratory of Nanodevices and Applications (grant number 13ZS02), Open Project of State Key Laboratory of Rare Earth Resource Utilizations (RERU2014010), Program for New Century Excellent Talents in University (NCET-13-0835), Henry Fok Education Foundation (141068) and Six Talents Peak Project in Jiangsu Province (XCL-025).

References

[1] P. Wang, P.-S. Yap, T.-T. Lim, C–N–S tridoped TiO2 for photocatalytic degradation of tetracycline under visible-light irradiation, *APPL. CATAL. A: GEN.*, 2011, **399**, 252-261.

[2] Y. Liu, X. Gan, B. Zhou, B. Xiong, J. Li, C. Dong, J. Bai, W. Cai, Photoelectrocatalytic degradation of tetracycline by highly effective TiO2 nanopore arrays electrode, *J. HAZRD. MATER.*, 2009, **171**, 678-683.

[3] X. Yu, Z. Lu, D. Wu, P. Yu, M. He, T. Chen, W. Shi, P. Huo, Y. Yan, Y. Feng, Heteropolyacid–chitosan/TiO2 composites for the degradation of tetracycline hydrochloride solution, *REACT. KINET. MECH. CAT.*, 2013, **111**, 347-360.

[4] X.D. Zhu, Y.J. Wang, R.J. Sun, D.M. Zhou, Photocatalytic degradation of tetracycline in aqueous solution by nanosized TiO2, *Chemosphere*, 2013, **92**, 925-932.

[5] C. Reyes, J. Fernández, J. Freer, M.A. Mondaca, C. Zaror, S. Malato, H.D. Mansilla, Degradation and inactivation of tetracycline by TiO2 photocatalysis, *J. PHOTOCH. PHOTOBIO: A.*, 2006, **184**, 141-146.

[6] X. Wu, Y. Wei, J. Zheng, X. Zhao, W. Zhong, The behavior of tetracyclines and their degradation products during swine manure composting, *BIORESOURCE.*

TECHNOL., 2011, **102** 5924-5931.

[7] R. Hao, X. Xiao, X. Zuo, J. Nan, W. Zhang, Efficient adsorption and visible-light photocatalytic degradation of tetracycline hydrochloride using mesoporous BiOI microspheres, *J. HAZARD. MATER.,* 2012, **209-210**, 137-145.

[8] X. Liu, P. Lv, G. Yao, C. Ma, P. Huo, Y. Yan, Microwave-assisted synthesis of selective degradation photocatalyst by surface molecular imprinting method for the degradation of tetracycline onto ClTiO2, *CHEM. ENG. J.,* 2013, **217**, 398-406.

[9] L.F. da Silva, J.-C. M'Peko, J. Andrés, A. Beltrán, L. Gracia, M.I.B. Bernardi, A. Mesquita, E. Antonelli, M.L. Moreira, V.R. Mastelaro, Insight into the Effects of Fe Addition on the Local Structure and Electronic Properties of SrTiO3, *J. PHYS. CHEM. C.*, 2014, **118**, 4930-4940.

[10] T. Puangpetch, T. Sreethawong, S. Yoshikawa, S. Chavadej, Synthesis and photocatalytic activity in methyl orange degradation of mesoporous-assembled SrTiO3 nanocrystals prepared by sol–gel method with the aid of structure-directing surfactant, *J. Mol. Catal. A: Chem.*, 2008, **287**, 70-79.

[11] M. Liu, X. Qiu, M. Miyauchi, K. Hashimoto, Energy-Level Matching of Fe(III) Ions Grafted at Surface and Doped in Bulk for Efficient Visible-Light Photocatalysts, *JACS*, 2013, **135**, 10064-10072.

[12] J. Li, S. Lv, Y. Liu, J. Bai, B. Zhou, X. Hu, Photoeletrocatalytic activity of an n-ZnO/p-Cu2O/n-TNA ternary heterojunction electrode for tetracycline degradation, *J. HAZARD. MATER.*, 2013, **262**, 482-488.

[13] T.-H. Xie, X. Sun, J. Lin, Enhanced photocatalytic degradation of RhB driven by visible light-induced MMCT of Ti(IV)-O-Fe(II) formed in Fe-Doped SrTiO3, *J. PHYS. CHEM. C.*, 2008, **112**, 9753-9759.

[14] M.L. Moreira, V.M. Longo, W. Avansi, M.M. Ferrer, J. Andrés, V.R. Mastelaro, J.A. Varela, É. Longo, Quantum Mechanics Insight into the Microwave Nucleation of SrTiO3Nanospheres, *J. PHYS. CHEM. C*., 2012, **116**, 24792-24808.

[15] S.D. Delekar, H.M. Yadav, S.N. Achary, S.S. Meena, S.H. Pawar, Structural refinement and photocatalytic activity of Fe-doped anatase TiO2 nanoparticles, *APPL SURF. SCI.*, 2012, **263**, 536-545.

[16] Q.I. Rahman, M. Ahmad, S.K. Misra, M. Lohani, Efficient Degradation of Methylene Blue Dye Over Highly Reactive Cu Doped Strontium Titanate (SrTiO3) Nanoparticles Photocatalyst Under Visible Light, *J. NANOSC.I NANOTECHNO.*, 2012, **12**, 7181-7186.

[17] V. Subramanian, R.K. Roeder, E.E. Wolf, Synthesis and UV-visible-light photoactivity of noble-metal-SrTiO3 composites, Industrial & Engineering Chemistry Research, *IND & ENG. CHEM. RES*. 2006, **45**, 2187-2193.

[18] J.-P. Zou, L.-Z. Zhang, S.-L. Luo, L.-H. Leng, X.-B. Luo, M.-J. Zhang, Y. Luo, G.-C. Guo, Preparation and photocatalytic activities of two new Zn-doped SrTiO3 and BaTiO3 photocatalysts for hydrogen production from water without cocatalysts loading, *INT. J HYDROGEN. ENERG.*, 2012, **37**, 17068-17077.

[19] A. Ghosh, M.G. Masud, J. Sannigrahi, B.K. Chaudhuri, Resistive transition, polaron dynamics and scaling behavior in Fe doped SrTiO3, *PHYS. REV. B*., 2013, **414**, 60-66.

[20] H.W. Kang, S.B. Park, Doping of fluorine into SrTiO3 by spray pyrolysis for H2 evolution under visible light irradiation, *CHEM. ENG. SCI.*, 2013, **100**, 384-391.

[21] H.-C. Chen, C.-W. Huang, J.C.S. Wu, S.-T. Lin, Theoretical Investigation of the Metal-Doped SrTiO3Photocatalysts for Water Splitting, *J. PHYS. CHEM. C.,*

2012, **116**, 7897-7903.

[22] K. Shan, X.-M. Guo, Electrical conduction behavior of A-site deficient (Y, Fe) co-doped SrTiO3 mixed ionic–electronic conductor, *MATER. LETT.,* 2013, **113**, 126-129.

[23] K. Žagar, C. Fàbrega, F. Hernandez-Ramirez, J.D. Prades, J.R. Morante, A. Rečnik, M. Čeh, Insight into the structural, electrical and photoresponse properties of individual Fe:SrTiO3 nanotubes, *MATER. CHEM. PHYS.*, 2013, **141**, 9-13.

[24] G. Neri, G. Micali, A. Bonavita, R. Licheri, R. Orrù, G. Cao, D. Marzorati, E. Merlone Borla, E. Roncari, A. Sanson, FeSrTiO3-based resistive oxygen sensors for application in diesel engines, *SENSOR. ACTUAT. B: CHEM.*, 2008, **134**, 647-653.

[25] J.J. Urban, W.S. Yun, Q. Gu, H. Park, Synthesis of single-crystalline perovskite nanorods composed of barium titanate and strontium titanate*, J. AM. CHEM. SOC*., 2002, **124**, 1186-1187.

[26] S. STEINSVIK, R. BUGGE, J. Gjønnes, J. TAFTØ, T. Norby, The defect structure of SrT1-xFexO3-y (x, *J. PHYS. CHEM. SOLIDS.*, 1997, **58**, 969-976.

[27] A. Rothschild, S.J. Litzelman, H.L. Tuller, W. Menesklou, T. Schneider, E. Ivers-Tiffée, Temperature-independent resistive oxygen sensors based on SrTi1−xFexO3−δ solid solutions, *SENSOR. ACTUAT. B: CHEM.,* 2005, **108**, 223-230.

[28] R. Yuan, B. Zhou, D. Hua, C. Shi, Enhanced photocatalytic degradation of humic acids using Al and Fe co-doped TiO2nanotubes under UV/ozonation for drinking water purification, *J. HAZARD. MATER*., 2013, **262**, 527–538.

[29] B. Gao, L. Liu, J. Liu, F. Yang, Photocatalytic degradation of

2,4,6-tribromophenol over Fe-doped ZnIn2S4: Stable activity and enhanced debromination, *APPL. CATAL. B: ENVIRON.*, 2013, **129**, 89-97.

[30] D. Yin, L. Zhang, K. Song, Y. Ou, C. Wang, B. Liu, and M. Wu, ZnO Nanoparticles Co^{-} Doped with Fe^{3+} and Eu^{3+} Ions for Solar Assisted Photocatalysis, J NANOSCI NANOTECHNO, 2014, **14**, 6077-6083.

[31] A.K. Sajjad, S. Shamaila, B. Tian, F. Chen, J. Zhang, Comparative studies of operational parameters of degradation of azo dyes in visible light by highly efficient WOx/TiO2 photocatalyst, *J. HAZARD. MATER.*, 2010, **177**, 781-791.

[32] X. Yan, B. Hu, W. Lu, S. Sun, W. Shi, X. Wang, Enhanced photocatalytic activity induced by surface plasmon resonance on Ag-loaded strontium titanate nanoparticles, Micro & Nano Letters, *MICRO. NANO. LETT.* 2013, **8**, 504-507.

[33] S. Sakiyama, S. Yamazoe, A. Uyama, M. Morimoto, S. Yokojima, Y. Kojima, S. Nakamura, K. Uchida, Photoinduced Reversible Heteroepitaxial Microcrystal Growth of a Photochromic Diarylethene on (110) Surface of SrTiO3, CRYST GROWTH DES, 2012, **12**, 1464−1468.

[34] Y. Wu, J. Zhang, L. Xiao, F. Chen, Preparation and characterization of TiO2 photocatalysts by Fe3+ doping together with Au deposition for the degradation of organic pollutants, *APPL. CATAL. B: ENVIRON.*, 2009, **88**, 525-532.

[35] J. Niu, S. Ding, L. Zhang, J. Zhao, C. Feng, Visible-light-mediated Sr-Bi2O3 photocatalysis of tetracycline: kinetics, mechanisms and toxicity assessment, *Chemosphere,* 2013, **93**, 1-8.

[36] K. Nagaveni, M.S. Hegde, G. Madras, Structure and photocatalytic activity of Ti1-xMxO2 +/-delta (M = W, V, Ce, Zr, Fe, and Cu) synthesized by solution combustion method, *J. PHYS. CHEM. B.*, 2004, **108**, 20204-20212.

[37] Y. Yan, Y. Wu, Y. Yan, W. Guan, W. Shi, Inorganic-Salt-Assisted Morphological Evolution and Visible-Light-Driven Photocatalytic Performance of Bi2WO6Nanostructures, *J. PHYS. CHEM. C*., 2013, **117**, 20017-20028.

[38] G. Zhang, W. Guan, H. Shen, X. Zhang, W. Fan, C. Lu, H. Bai, L. Xiao, W. Gu, W. Shi, Organic Additives-Free Hydrothermal Synthesis and Visible-Light-Driven Photodegradation of Tetracycline of WO3 Nanosheets, *IND. ENG. CHEM. RES.*, 2014, **53**, 5443-5450.

[39] U.A. Joshi, J.R. Darwent, H.H.P. Yiu, M.J. Rosseinsky, The effect of platinum on the performance of WO3 nanocrystal photocatalysts for the oxidation of Methyl Orange and iso-propanol, *J. CHEM. TECHNOL. BIOT*., 2011, **86**, 1018-1023.

[40] S. Liu, N. Zhang, Z.-R. Tang, Y.-J. Xu, Synthesis of One-Dimensional CdS@TiO2Core–Shell Nanocomposites Photocatalyst for Selective Redox: The Dual Role of TiO2Shell, *ACS. APPL. MATER. INTER.*, 2012, **4**, 6378-6385.

[41] X. Wang, K. Maeda, X. Chen, K. Takanabe, K. Domen, Y. Hou, X. Fu, M. Antonietti, Polymer Semiconductors for Artificial Photosynthesis: Hydrogen Evolution by Mesoporous Graphitic Carbon Nitride with Visible Light, *J. AM. CHEM. SOC.,* 2009, **131**, 1680-1684.

[42] L. Ye, J. Liu, C. Gong, L. Tian, T. Peng, L. Zan, Two Different Roles of Metallic Ag on Ag/AgX/BiOX (X = Cl, Br) Visible Light Photocatalysts: Surface Plasmon Resonance and Z-Scheme Bridge, *ACS. CATAL.*, 2012, **2**, 1677-1683.

[43] T.B. Li, G. Chen, C. Zhou, Z.Y. Shen, R.C. Jin, J.X. Sun, New photocatalyst BiOCl/BiOI composites with highly enhanced visible light photocatalytic performances, *DALTON. T.*, 2011, **40**, 6751-6758.

[44] S.C. Yan, Z.S. Li, Z.G. Zou, Photodegradation of rhodamine B and methyl orange over boron-doped g-C3N4 under visible light irradiation, Langmuir : *the*

ACS journal of surfaces and colloids, 2010, **26**, 3894-3901.

[45] X. Lu, Y. Ma, B. Tian, J. Zhang, Preparation and characterization of Fe–TiO2 films with high visible photoactivity by autoclaved-sol method at low temperature, *SOLID. STATE. SCI.,* 2011, **13**, 625-629.

[46] L. Wang, Y. Yao, L. Sun, Y. Mao, W. Lu, S. Huang, W. Chen, Rapid removal of dyes under visible irradiation over activated carbon fibers supported Fe(III)–citrate at neutral pH, SEP PURIF TECHNOL., 2014, **122**, 449–455.

[47] Y. Y, W. L, S. L, Z. S, H. Z, W. Lu, Y. M,Chen W, Efficient removal of dyes using heterogeneous Fenton catalysts based on activated carbon fibers with enhanced activity, Chemical Engineering Science, 2013, **101**, 424-431.

[48] J. Shu, Z. Wang, G. Xia, Y. Zheng, L. Yang , W. Zhang, One-pot synthesis of AgCl@Ag hybrid photocatalyst with high photocatalytic activity and photostability under visible light and sunlight irradiation, *CHEM. ENG. J.,* 2014, **252**, 374–381.

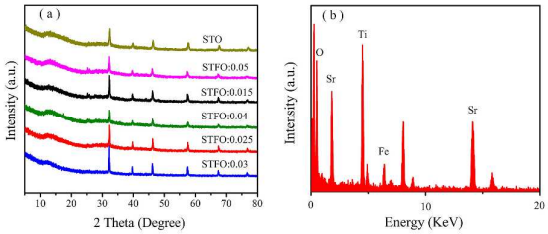

Fig. 1. (a) XRD patterns of obtained samples with different Fe^{3+} proportion; (b) EDX spectrum of FSTO: 0.03.

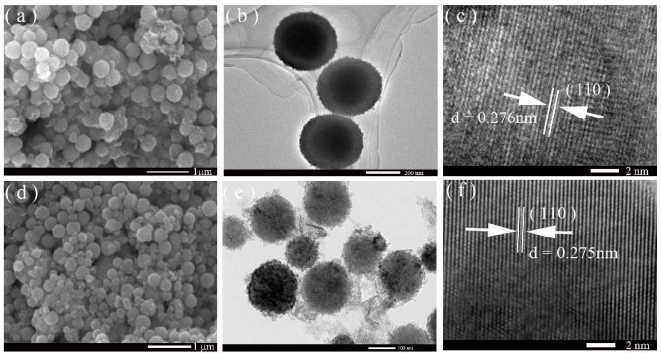

Fig. 2. SEM images of pure STO (a) and FSTO: 0.03(d); TEM images of pure STO (b) and FSTO: 0.03(e); HRTEM images of pure STO (c) and FSTO: 0.03(f)

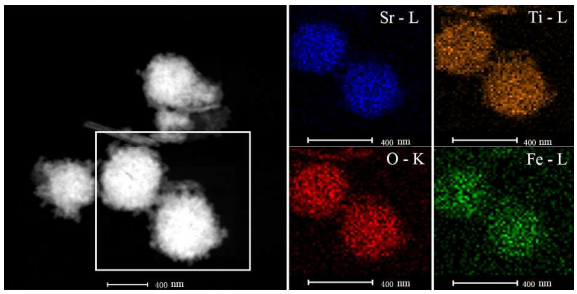

Fig. 3. HAADF-STEM images of the FSTO: 0.03 sample with maps of Sr–L, Ti–L, O–K and Fe–L.

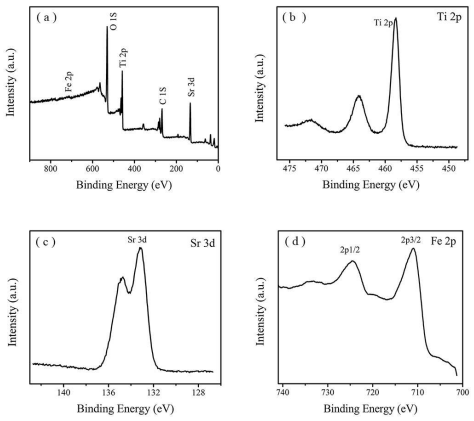

Fig. 4. (a) The full range XPS spectrum; (b-d) the high-resolution XPS spectra of Sr, Ti and Fe respectively of FSTO: 0.03 sample.

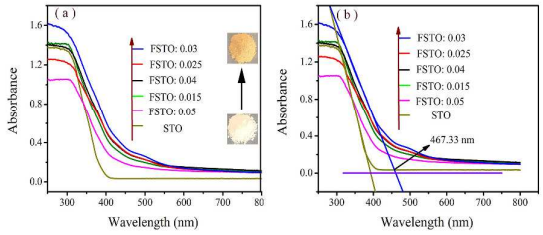

Fig. 5. UV-vis diffuses reflectance spectra of different samples with color contrast in photos (inset).

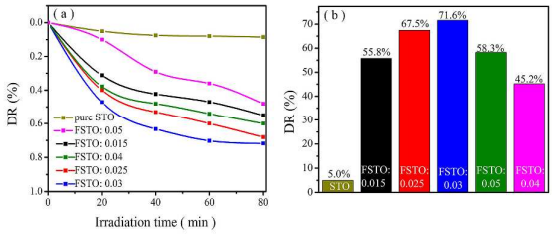

Fig. 6. Photocatalytic degradation ratios of TC with different samples under visible light irradiation.

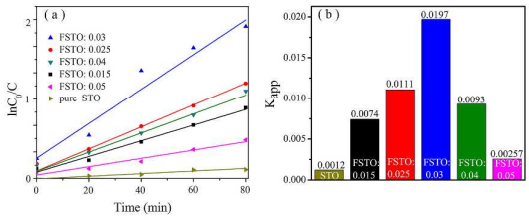

Fig. 7. (a) The first-kinetic of the photocatalytic degradation of TC; (b) Apparent rate constant values for photodegradation of the TC solution over different photocatalysts in 80 min under visible light irradiation.

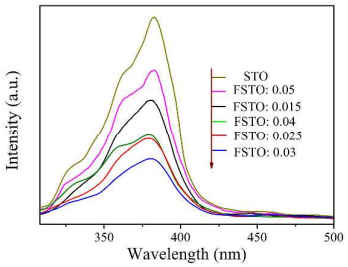

Fig. 8. PL spectrum of different samples with the excitation wavelength of 281 nm.

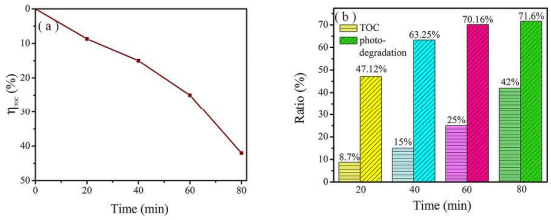

Fig. 9. The TOC removal curves of FSTO: 0.03 under visible light irradiation (a); degradation curve trend contrasts tetracycline and TOC in 80 min (b).

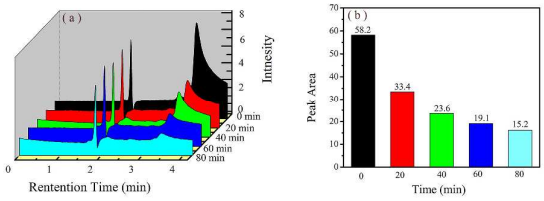

Fig. 10. High-performance liquid chromatography (HPLC) analyses of TC photodegradation over FSTO: 0.03 under visible light irradiation (a); the peak area which represents the relative concentration of TC (b).

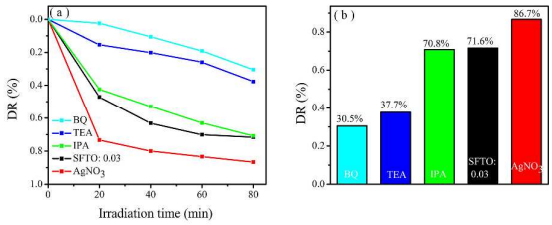

Fig. 11. Photocatalytic degradation ratios of TC using different radical scavengers over FSTO: 0.03 under visible light irradiation for 80 min.

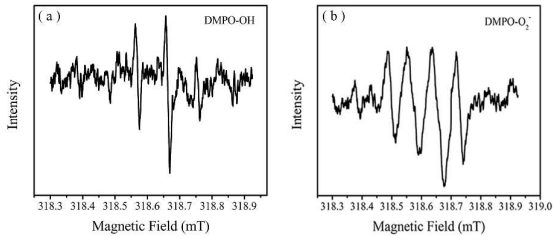

Fig. 12. DMPO spin-trapping ESR spectra of TC solutions after visible light irradiation ((a) FSTO: 0.03- H2O/DMPO, (b) FSTO: 0.03-CH3OH/DMPO).

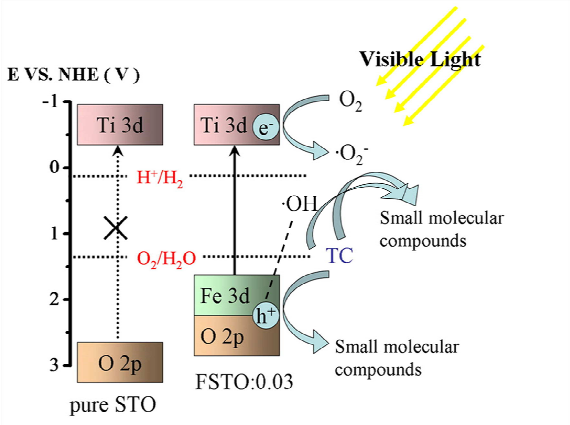

Scheme 1. Mechanistic pathway of electrons and holes under visible light illumination over FSTO: 0.03 photocatalysts.

Table captions

Table 1. The proportion of elements of FSTO: 0.03.

Element	Atomic %
Sr3d Scan	16.85
C1s Scan	10.99
Ti2p Scan	16.06
O1s Scan	55.1
Fe2p Scan	1.0